



Detection of chromospheric magnetic fields: a forward modeling approach

H. Uitenbroek

National Solar Observatory/Sacramento Peak, Sunspot, NM 88349, USA
e-mail: hui.tenbroek@nso.edu

Abstract. We show that circular and linear polarization in chromospheric spectral lines, in particular that resulting from the Zeeman effect, is generally expected to be small because these lines form at high temperatures and arise from light elements. To illustrate these points we solve two-dimensional non-LTE radiative transfer in the Ca II 854.21 nm line through a magnetostatic flux concentration model and calculate the expected polarization. Finally, we show that the vertical magnetic field on the axis of the concentration can be recovered by measuring the bisector separation of the left- and right-hand circularly polarized emergent profiles.

Key words. Sun: chromosphere – magnetic fields – line: profiles – radiative transfer – polarization

1. Introduction

Simulations of the structure and dynamics of the solar chromosphere have advanced to sufficient realism that it is now becoming possible and essential to test them against detailed observations (see the contributions by Carlsson, Hansteen, Leenaarts, and Abbett in these proceedings). Perhaps the most important quantity to be measured is the chromospheric magnetic field structure, because it becomes the dominant force in these atmospheric layers. In addition, much of the chromospheric heating seems to be coincident with the presence of magnetic fields. Unfortunately, the magnetic field vector in the chromosphere is hard to determine for at least two reasons. First, the field is intrinsically weak because it can no longer be contained by gas pressure at the low densi-

ties that prevail in the chromosphere, in contrast to the high-field concentrations that are maintained by the much greater densities in the photosphere. Secondly, in the Zeeman regime the polarization signals in chromospheric lines are relatively weak because these lines form at high temperatures, hence with large thermal widths, and consequently, small ratios of line splitting over Doppler broadening. This particularly affects the linear polarization signal, which, in the weak field limit, is proportional to the square of this ratio.

In this contribution I investigate the magnitude of polarization signals that can be expected in the Ca II 854.21 nm infrared triplet line from the Zeeman effect through a relatively simple magneto-static flux concentration model that extends into the chromosphere. The signals in all four Stokes parameters are calculated with full two-dimensional non-LTE,

Send offprint requests to: H. Uitenbroek

multi-level, polarized radiative transfer, using the thermal and magnetic structure of the model. This forward modeling of the polarized transfer in a horizontally structured model is complementary to spectral-line inversions, which typically analyze the spectrum on a column-by-column basis, and do not allow the investigation of multi-dimensional transfer effects. In addition, whereas inversions are essentially results-driven, this exercise is also meant to understand the radiative transfer and diagnostic capabilities of the Ca II 854.21 nm line.

2. Polarized radiative transfer in chromospheric spectral lines

In the absence of polarization emitting or absorbing material, the equation of transfer is a simple first-order differential equation for the scalar intensity I . In the presence of magnetic fields, atoms may change the polarization state of the radiation field through absorption and emission. In this case, we have to account for the transfer of all four Stokes parameters, as well as the cross-talk between them. The equation of transfer for four component Stokes vector \mathbf{I} along length s now becomes:

$$\frac{d\mathbf{I}}{ds} = -\mathbf{K}\mathbf{I} + \mathbf{j}, \quad (1)$$

where $\mathbf{I} = (I, Q, U, V)^\dagger$, $\mathbf{j} = (j_c + j_l\Phi)\mathbf{e}_0$, $\mathbf{e}_0 = (1, 0, 0, 0)^\dagger$ is the combined emissivity of continuum and line, and $\mathbf{K} = \alpha_c\mathbf{1} + \alpha_l\Phi$ is the 4×4 absorption matrix, with the continuum and line absorption coefficients α_c and α_l , respectively.

The 4×4 absorption matrix Φ contains elements $\phi_{I,Q,U,V}$ that describe the interaction between Stokes I and the polarization states Q , U , and V , and elements $\psi_{Q,U,V}$ that describe the cross-talk between the polarization states. The elements ϕ have the following structure:

$$\begin{aligned} \phi_I &= \phi_\Delta \sin^2 \gamma + \frac{1}{2}(\phi_+ + \phi_-) \\ \phi_Q &= \phi_\Delta \sin^2 \gamma \cos 2\chi \\ \phi_U &= \phi_\Delta \sin^2 \gamma \sin 2\chi \\ \phi_V &= \frac{1}{2}(\phi_+ - \phi_-) \cos \gamma, \quad \text{with:} \end{aligned} \quad (2)$$

$$\phi_\Delta = \frac{1}{2} \left[\phi_0 - \frac{1}{2}(\phi_+ + \phi_-) \right],$$

(see Landi Degl'Innocenti & Landolfi, 2004, p. 387) where the angles γ and χ specify the inclination and azimuth, respectively, of the magnetic field with the line of sight. Similar expressions are found for the elements ψ of Φ , but we will concentrate on the expressions for $\phi_{I,Q,U,V}$ here. In the case of the Zeeman effect, these quantities contain the unshifted ($\phi_0, \Delta m = 0$) and shifted ($\phi_\pm, \Delta = \pm 1$) Zeeman components (for simplicity in the case of a Zeeman triplet, but similar expressions apply in the general case):

$$\begin{aligned} \phi_0 &= H(a, v + v_{\text{los}}) \\ \phi_\pm &= H(a, v \pm v_{\text{B}} + v_{\text{los}}) \\ H(a, v) &= \frac{a}{\pi} \int_{-\infty}^{\infty} \frac{\exp(-y^2)}{(v-y)^2 + a^2} dy \end{aligned} \quad (3)$$

with $H(a, v)$ the normalized Voigt function and the line-of-sight velocity v_{los} and Zeeman shift v_{B} , both in Doppler units, and the Doppler width λ_{D} given by:

$$\begin{aligned} v_{\text{los}} &= \lambda \frac{\mathbf{v} \cdot \mathbf{n}}{c\Delta\lambda_{\text{D}}} \\ \Delta\lambda_{\text{D}} &= \frac{v_{\text{broad}}\lambda}{c} \\ v_{\text{broad}} &= \sqrt{2kT/m} \\ v_{\text{B}} &= g_L \frac{e\lambda^2 B}{4\pi m_e c \Delta\lambda_{\text{D}}} \end{aligned} \quad (4)$$

In these equations λ is the central wavelength of the line, m the mass of the atomic species, e and m_e , the charge and mass of the electron, respectively, and T is the kinetic temperature. It is important to note that the Zeeman splitting v_{B} , in Doppler units, depends on the temperature T and mass of the atomic species m through the Doppler width $\Delta\lambda_{\text{D}}$. For larger temperatures and smaller atomic masses, the line splitting in terms of Doppler units becomes smaller.

When the temperature is high enough, the magnetic field B is weak enough, and the atom is light enough, the weak-field approximation applies ($v_{\text{B}} \ll 1$ so that we can realistically

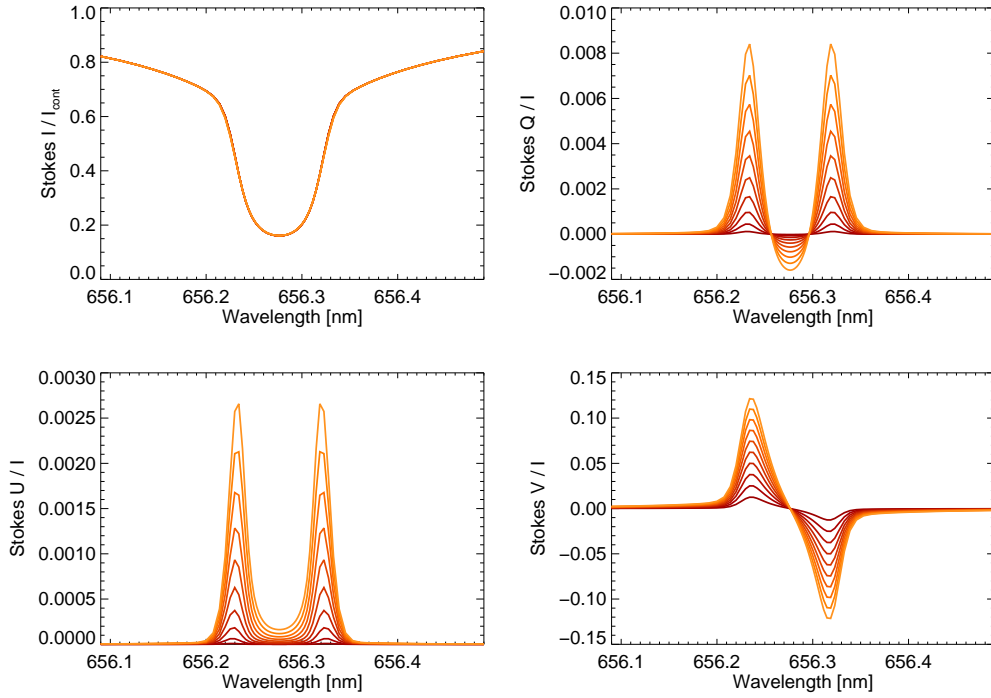


Fig. 1. Stokes profiles in the hydrogen $H\alpha$ line for field strengths of 200 to 2000 G. The field in each case was constant with height, and at an angle of 45° with the vertical line of sight. The field azimuth was 90° . Profiles were calculated with full non-LTE polarized radiative transfer, not using the weak field approximation.

approximate the Voigt function with the first two terms of its Taylor expansion:

$$H_{\pm} \approx H_0 \mp v_B \frac{\partial H_0}{\partial v} + \frac{1}{2} v_B^2 \frac{\partial^2 H_0}{\partial v^2}. \quad (5)$$

In this case, using the expressions given in Eq. 3, we find that:

$$\phi_V \propto v_B \frac{\partial H_0}{\partial v} \quad (6)$$

$$\phi_{Q,U} \propto v_B^2 \frac{\partial^2 H_0}{\partial v^2} \quad (7)$$

In particular, Eq. 7 shows that the polarization that results from the transverse Zeeman effect is reduced for small v_B . We demonstrate this in practice in Fig. 1, where we show the Stokes I, Q, U, V profiles in the hydrogen $H\alpha$ line calculated in the vertical direction

through the standard FAL C model atmosphere (Fontenla et al., 1993) with different constant magnetic field strengths ranging from 200 to 2000 G. Note in particular the very small values of the net linear polarization measures Q and U . By comparison, the linear polarization fractions Q/I and U/I reach 0.17 in the Fe I 630.25 nm line with the same magnetic field configuration, because iron is a much heavier atom, and because the line forms in the photosphere at much lower temperature than $H\alpha$. The linear polarization fractions in the likewise chromospheric Ca II 854.21 nm line reach 0.04 and 0.02, substantially above the values in $H\alpha$ because calcium is about 40 times heavier than hydrogen. Considering the sensitivity of the emergent polarization profiles to temperature and atomic mass, it is clear that we cannot expect large linear polarization signals

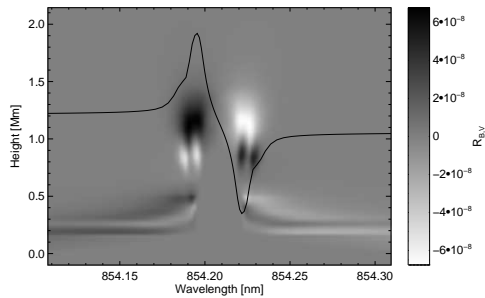


Fig. 2. Response function $R_{V,B}$ of the 854.21 nm Stokes V profile, which is overplotted in black, to perturbations in the magnetic field strength B . $R_{V,B}$ was calculated by perturbing a 10^3 G vertical magnetic field by 1% in standard 1-D hydrostatic solar model. The Stokes V profile in this line is most sensitive to the field at a height of about 1 Mm in such a model.

from the transverse Zeeman effect in chromospheric lines, which on average form at relatively high temperatures, and which (in the visible) all happen to arise from light elements like hydrogen, magnesium, sodium and calcium.

3. The polarization signal in a flux concentration

3.1. The calcium 854.21 nm line

At the temperatures and densities in the solar photosphere and chromosphere, calcium appears predominantly in its singly ionized state. Since calcium is a relatively abundant element, the lines in the lower part of the term diagram of this state are among the strongest in the visible part of the solar spectrum. The 854.21 nm line is of the Ca II infrared triplet (IRT) lines that connect the $3d^2D$ (lower) and $4p^2P$ (upper) levels radiatively. The $3d$ levels are metastable (i.e., there is no dipole radiative transition to the $3s^2S$ ground level), and are therefore long lived and well populated providing ample opacity in the 854.21 nm line. This line also shares its upper level with K resonance line, the strongest line in the visible solar spectrum. While the $H\alpha$ line has little sensitivity to conditions in the temperature mini-

mum because the relatively low temperatures there are insufficient to excite hydrogen over the 10.3 eV from the ground level to the first excited state (the $H\alpha$ lower level), the 854.21 lower level is well populated by collisional excitation from the Ca II ground level throughout this region. The line therefore shows much more sensitivity to conditions in lower temperature regions than the $H\alpha$ line, even though hydrogen is roughly 5×10^5 times more abundant.

The sensitivity of the circular polarization in the 854.21 nm line to the magnetic field in the chromosphere is demonstrated in Fig. 2 with a graph of the response function of Stokes V in that line to changes in the field strength. The complexity of the response function, with positive and negative values at different heights for the same wavelength, stems from the shape of the 854.21 source function in the employed atmospheric model, which decreases with height in the photosphere, rises to a relative maximum at about 1 Mm, and then drops off again. When the magnetic field perturbations slightly increase the line splitting, the formation of the line moves down in the atmosphere to higher or lower values of the source function, and higher or lower values of the emergent intensity at a given wavelength, giving rise to a positive or negative response function depending on the slope of the source function at the formation height of that wavelength.

3.2. The flux concentration model

To investigate the feasibility of determination of the chromospheric magnetic vector field through measurement of the polarization from the Zeeman effect in the Ca II 854.21 nm line we solve the radiative transfer for the full Stokes vector in a two-dimensional magnetostatic model of a flux concentration. The model was constructed by imposing a thermal stratification on both the concentration axis (FAL model F, representative of solar plage) and the exterior (model FAL A, representative of a cool super granulation cell interior). A Wilson depression was applied to the interior atmosphere so that the canopy, the height where the magnetic field can no longer be contained by the in-

ternal pressure, occurred at 1 Mm, given the diameter and the field strength of the concentration in the photosphere. The solution of magnetostatic equilibrium was iterated with a full two-dimensional non-LTE solution of hydrogen radiative transfer to get the electron density consistent with ionization in hydrogen, given the multi-dimensional thermal structure of the flux concentration model. This included Partial frequency redistribution (PRD) in the Lyman α line, which is necessary to correctly estimate the amount of downward radiation in the wings of this line, which in turn determines the population of the first excited level in hydrogen from which most ionization in hydrogen takes place through the Balmer continuum. The flux concentration in the particular model employed here has a field strength of approximately 2700 G in the photosphere with a radius of 170 km there, expanding to 5000 km at the canopy height and above. Figure 3 shows the resulting magnetic field strength and inclination. It is clear from the upper panel in this figure that the field strength drops very quickly with height to only about 10 G once the field expands very rapidly with height at the level of the canopy.

To compute the emergent polarization signals in the Ca II 854.21 nm line, non-LTE ra-

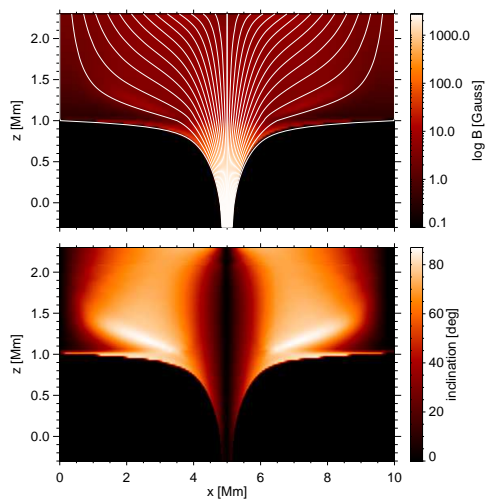


Fig. 3. Magnetic field strength (upper panel and inclination lower panel).

diative transfer was solved in a 5-level plus continuum atom that included the H and K resonance lines (both in PRD), the three IRT lines, and radiative bound-free transitions. The transfer solution in the two-dimensional model was performed with a Multi-Level Accelerated Lambda Iteration (MALI) code based on the Rybicki & Hummer (1992) formalism adapted to PRD by Uitenbroek (2001). Given the population numbers from the two-dimensional non-LTE solution, the full Stokes vector was then calculated for this solution, under the assumption that the magnetic field in the model is too weak everywhere in the model to influence the radiative rates in any of the 5 bound-bound transitions, which is a good assumption given the width of all included lines.

3.3. Results

The spatially resolved Stokes profile V/I emerging in the vertical direction is shown in Fig. 4. It is clear from this figure that the Stokes signal is mostly confined to the photospheric diameter of the flux concentration, which is outlined by the dashed vertical lines. Indeed, by the time the flux concentration expands above the canopy the field strength on its axis drops to about 10 G at 1 Mm and keeps dropping to 2 G at the top of the box at 2.3 Mm. As a result the amplitude of the V/I signal in the 854.21 nm line on the flux concentration axis corresponds to that of an FAL F atmosphere (the thermal model on the axis) with a constant vertical field of only 50 G, because the Stokes V signal near the core of the line is weighted to chromospheric layers at around 1 Mm (see Fig. 2). However, the actual emergent Stokes profile on the flux concentration axis has much broader lobes because further away from line center the intensity forms much deeper in the atmosphere, where the Zeeman splitting is much larger due to the field strengths in the kilo-Gauss range lower down.

The total circular polarization (defined as the wavelength integrated absolute value of V/I) in the Ca II 854.21 line across the flux concentration is given in Fig. 5. It reaches a maxi-

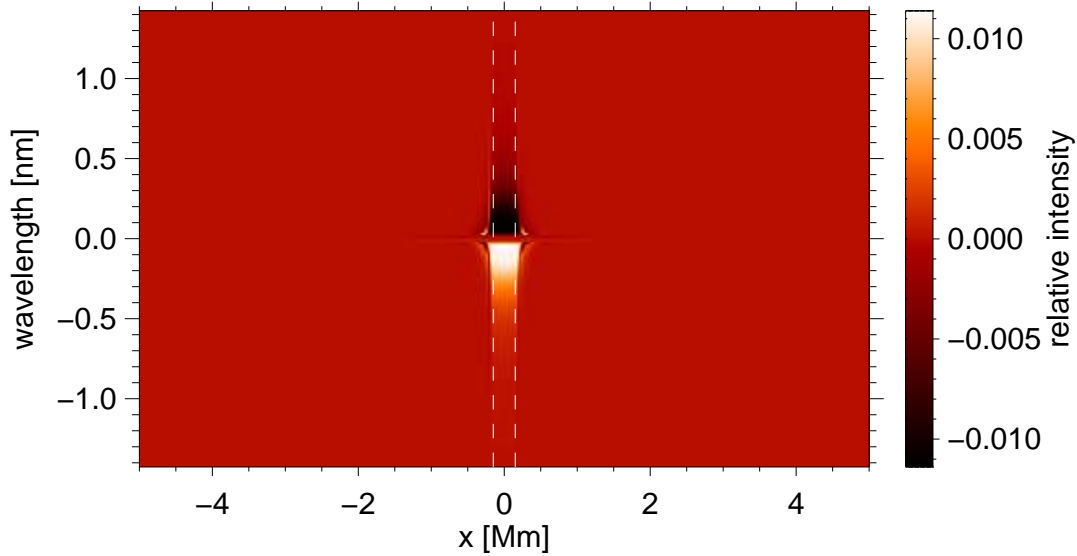


Fig. 4. The spatially resolved fraction of circular polarization V/I in the vertical direction across the flux concentration. Dashed vertical lines indicate the photospheric boundary of the concentration.

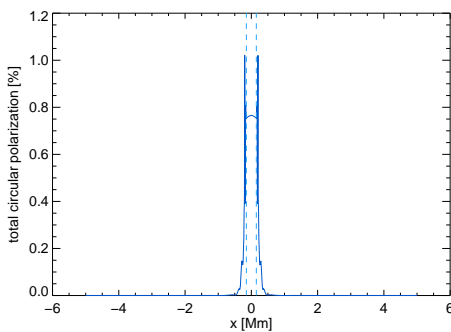


Fig. 5. Total circular polarization across the magnetic flux concentration.

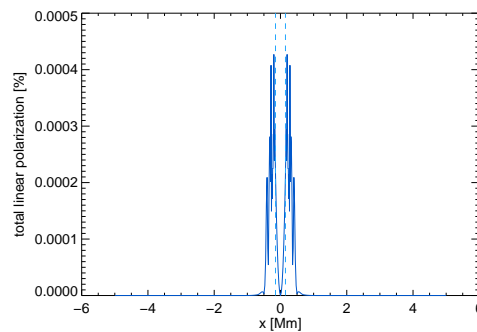


Fig. 6. Total linear polarization across the magnetic flux concentration.

imum value of about 1% right over the flux concentration (the photospheric boundary of the flux concentration is delineated by the two vertical dashed lines), and decreases rapidly outside of this area. With the rapid expansion of the flux concentration above the canopy, the field becomes so attenuated that it contributes very little to the circular polarization emerging in the vertical direction, even when the fields

are mostly in the direction of the line of sight in the higher layers.

The total linear polarization, taken as the wavelength integrated value of $\sqrt{(Q/I)^2 + (U/I)^2}$, for the 854.21 nm line across the flux concentration is shown in Fig. 6. Like the total circular polarization the total linear polarization is strongly peaked, but its values are several orders of magnitude smaller. The reasons for this are twofold: the fields

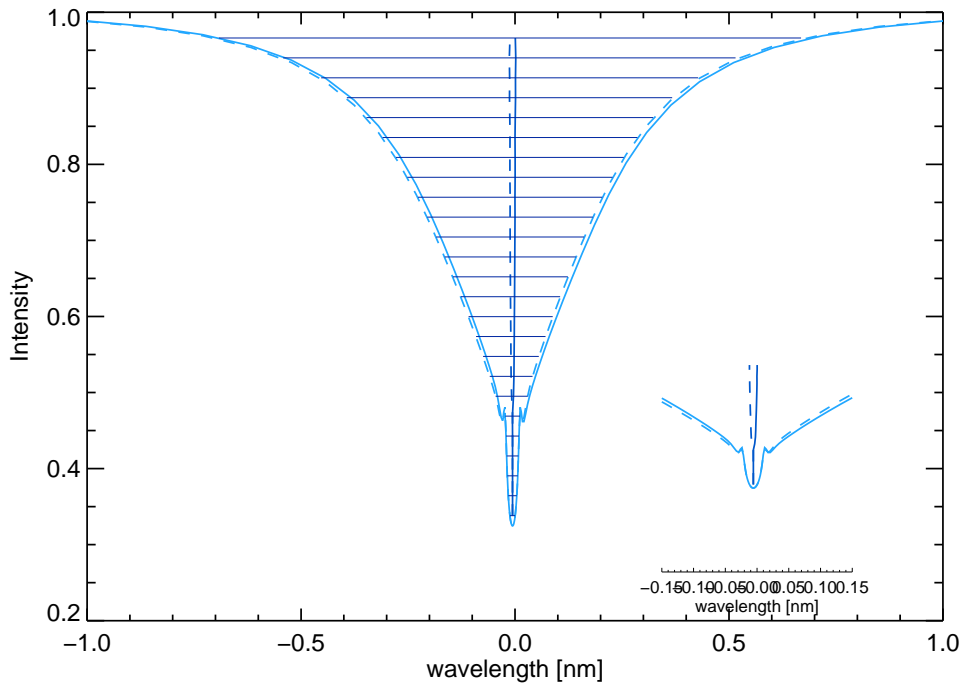


Fig. 7. Profiles and bisectors of the left- and right-hand circular polarization on the axis of the flux concentration. Horizontal lines mark the intensity levels at which the bisectors were determined.

reach substantial inclinations only where they are already weak (see Fig. 3, bottom panel), and the linear polarization is second order in the ratio of Zeeman splitting over Doppler width, which is a small number in a chromospheric line like 854.21 nm (see Eqs. 5 and 7). The strongest fields with high inclination occur along the walls of the concentration close to the axis (see Fig. 3, bottom panel). These give rise to the highest linear polarization values, just outside the photospheric tube borders. Inside the tube, near the axis the field is strictly vertical, which gives rise to zero linear polarization from the transverse Zeeman effect. The very small amount of linear polarization (at most 4×10^{-6}) predicted by the current model would be very hard to measure in practice, in particular because these small-scale flux elements are very dynamic in the real Sun, so that long integration times cannot be afforded.

3.4. Recovering the line-of-sight field strength

In the context of the flux concentration model we employ, it is clear from the previous sections that it would be very hard to recover the full chromospheric vector field observationally, mainly because the linear polarization signal is too small. But what about the line-of-sight field strength? In the current model the field gradient with height is particularly large because of the strong expansion of the field above 1 Mm. It is reasonable to assume that this will also be the case for flux concentrations in relatively quiet areas of the real Sun. Such strong gradients make determination of the field strength with “one-point” measurements like a Milne-Eddington inversion, or center-of-gravity determination (Rees & Semel, 1979; Uitenbroek, 2003) unreliable, because they are

weighted too much to the strong field in the photosphere, which causes much larger splitting in the wings than in the core of the line. To get more resolution in height it is advantageous to measure the bisectors of both the right- and left-hand circular polarization (i.e., $I + V$ and $I - V$) at different depths in the line. The differences between these two bisectors then provide a measure for the Zeeman splitting at different positions in the line, and therefore for different heights in the atmosphere. In practice this is a difficult measurement when real observations with noise are considered (see the contribution by Wöger et al. in these proceedings), but we explore the theoretical measurement here in the following section.

Figure 7 shows the line profiles and bisectors for the emergent left- and right-handed circular polarization in the vertical direction for the location of the axis of the flux concentration ($x = 0$, see Fig. 4). The inset in this figure makes clear that the bisector separation becomes very small in the core of the line because of the low field strength at the heights at which the core of the line forms. Further into the line wings the separation increases, reflecting the increase of field strength with depth in the atmosphere.

For each intensity level marked in Fig. 7 the line-of-sight magnetic field strength can be found from (e.g., Stenflo, 1994, p. 111):

$$B_{\text{LOS}} = \frac{\lambda_+ - \lambda_-}{2} \frac{4\pi m_e c}{e g_L \lambda_0^2}. \quad (8)$$

where λ_{\pm} are the bisectors of the left- and right-hand polarized profile, λ_0 and g_L are the central wavelength and Landé factor of the 854.21 nm line, respectively, and m_e and e are the mass and charge of the electron. To assign a height to each B_{LOS} measurement, the geometrical height of $\tau_{\lambda} = 1$ at the wavelength where the pertinent intensity level intersects the line profile was determined. The resulting values are plotted in Fig. 8 along with the actual field strength on the axis of the concentration. The run of actual field strength with height is reasonably well recovered by this estimate. However, the same method provides a much less accurate measurement of the field away from the axis, because the field is weaker,

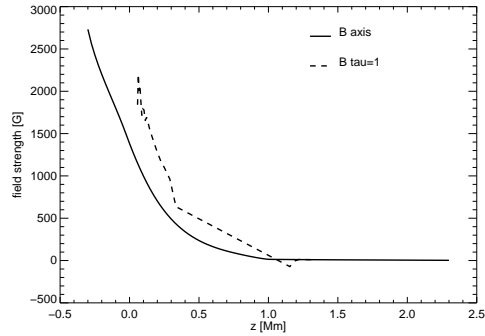


Fig. 8. Actual field strength on the axis of the flux concentration, and the field strength recovered from measuring the separation of bisectors of the left- and right-hand circularly polarized emergent line profiles (dashed curve).

and because the discontinuity of the canopy cannot be resolved.

4. Conclusion

We have shown that chromospheric spectral lines are expected to have smaller polarization signals than their photospheric counter parts because they typically arise from lighter elements and form at higher temperatures. Both factors contribute to a small ratio of line splitting to Doppler width. In the weak-field limit, circular polarization resulting from the Zeeman effect is proportional to this ratio, and linear polarization from the transverse Zeeman effect is proportional to the square of this ratio. The latter is therefore particularly small for chromospheric lines, making determination of the full vector field hard. Moreover, chromospheric fields (outside sunspots) are in general much weaker than in the photosphere, making them even harder to observe via the Zeeman effect. We have shown that the linear polarization that can be expected in the Ca II 854.21 nm line from our magnetostatic flux concentration is extremely small. The field strength on the tube axis can, in theory, be reasonably well recovered from measurement of the separation of bisectors of the left- and right-hand circularly polarized line profiles, despite the strong gradient of the field with height.

While the measurement of photospheric magnetic fields via the Zeeman effect is well established now, and feasible to a high degree of accuracy with current instrumentation and techniques, the same cannot be expected for chromospheric fields. With the small polarization signals that we expect, significantly larger telescopes will be needed to achieve the required polarimetric sensitivity on small spatial scales and at short time scales. Other techniques, employing for instance Hanle depolarization, may prove to be more fruitful for chromospheric magnetic field measurement than the Zeeman effect (see the contribution by Trujillo Bueno in these proceedings)

References

- Fontenla, J. M., Avrett, E. H., & Loeser, R. 1993, *ApJ*, 406, 319
- Landi Degl'Innocenti, E. L. & Landolfi, M. 2004, *Polarization in Spectral Lines* (Dordrecht, The Netherlands: Kluwer Academic Publishers)
- Rees, D. E. & Semel, M. D. 1979, *A&A*, 74, 1
- Rybicki, G. B. & Hummer, D. G. 1992, *A&A*, 262, 209
- Stenflo, J.-O. 1994, *Solar Magnetic Fields. Polarized Radiation Diagnostics* (Dordrecht: Kluwer Academic Publishers)
- Uitenbroek, H. 2001, *ApJ*, 557, 389
- Uitenbroek, H. 2003, *ApJ*, 592, 1225